Fitting Out-of-Focus Star Images to Measure the Focus and Alignment of the Dark Energy Camera

Gary A. Binder

Office of Science, Science Undergraduate Laboratory Internship (SULI) Program

California Institute of Technology

SLAC National Laboratory

Menlo Park, California

August 13, 2009

Prepared in partial fulfillment of the requirements of the Office of Science, Department of Energy's Science Undergraduate Laboratory Internship under the direction of Aaron Roodman at the Kavli Institute for Particle Astrophysics and Cosmology, SLAC National Laboratory

Participant: _____

Research Adviser: _____

Work supported in part by US Department of Energy contract DE-AC02-76SF00515.

Contents

Abstract

Fitting Out-of-Focus Star Images to Measure the Focus and Alignment of the Dark Energy Camera. GARY A. BINDER (California Institute of Technology, Pasadena, CA 91125) AARON ROODMAN (SLAC National Laboratory, Menlo Park, CA 94204)

In order to make accurate measurements of dark energy, a system is needed to monitor the focus and alignment of the Dark Energy Camera (DECam) to be located on the Blanco 4m Telescope for the upcoming Dark Energy Survey. One new approach under development is to fit out-of-focus star images to a point spread function from which information about the focus and tilt of the camera can be obtained. As a first test of a new algorithm using this idea, simulated star images produced from a model of DECam in the optics software Zemax were fitted. Then, real images from the Mosaic II imager currently installed on the Blanco telescope were used to investigate the algorithm's capabilities. A number of problems with the algorithm were found, and more work is needed to understand its limitations and improve its capabilities so it can reliably predict camera alignment and focus.

Introduction

The Dark Energy Survey represents an international effort to investigate the nature of the mysterious accelerated expansion of the universe, commonly attributed to a dark energy that permeates all space. The main goal of the survey is to measure the parameter w appearing in the equation of state for dark energy. To accomplish this goal, the survey will use the 4 meter Victor M. Blanco Telescope at the Cerro Tololo Inter-American Observatory in Chile, and a camera specifically designed for this purpose, the Dark Energy Camera (DECam). Approximately 300 million galaxies over 5 years will be imaged across 5000 square degrees of the southern sky. The astronomical methods used to measure dark energy include galaxy cluster counts, baryon oscillations, supernovae, and weak gravitational lensing. Critical to the accuracy of these measurements is a sound understanding of the physical limitations of the telescope and camera optics due to atmospheric distortion, camera alignment and focus, and imperfections in the CCDs (charged-coupled devices) used to capture images, among other things. This is particularly important for weak gravitational lensing measurements; understanding how images are affected by the above effects is essential to get accurate results.[1] A variety of systems are in place to understand and counteract optical systematic effects.

One particular system involves the focus and alignment sensors located on the periphery of the focal plane of DECam. These are 8 2k $\times$ 2k CCDs located alternately above and below the optimal focal plane of DECam by 1.5 millimeters as shown in Figure 1.[2] The CCDs will image stars and provide information on the positioning of the camera with respect to the primary mirror axis of the telescope. Because of fluctuations in the mechanical structure supporting the camera, small displacements in camera position are expected along the 6 degrees of freedom of the camera (3 in rotation and 3 in position). A hexapod system can maneuver the camera to correct for these fluctuations, using information provided by the focus and alignment sensors on the focal plane as well as from other monitoring systems. A fitting algorithm is under development that will take star images from the focus and alignment CCDs and provide information on the tilt of the camera, its position along the axis of the telescope i.e. how well in focus it is, and other relevant parameters to be discussed later. The primary purpose of the project was to test this new algorithm, first with artificial images made with the aid of the optics simulation software *Zemax*, and secondly with real images from the Mosaic II imager currently installed on the telescope. The results of the fits were compared against expected values, improvements were implemented, and problems noted.

Methods

The primary tools of investigation were all computer-based. Perhaps the most valuable tools for analysis of the reliability of the algorithm were the models of the Blanco Telescope, Dark Energy Camera, and the

Mosaic II imager in *Zemax*. A diagram taken from *Zemax* illustrates the model of DECam and the Blanco Telescope in Figure 2. With these models, a procedure was devised to create artificial images to be used in the first test. *Zemax* performs ray tracing on the model the user creates to determine many useful quantities and functions describing the optical system. Among these are the point spread function (PSF), wavefront map, and Zernike coefficients. The PSF represents the image of a hypothetically infinitely distant point source at a chosen plane in the optical system. Since stars are so distant, the PSF effectively represents the image of a star at the chosen location in the camera, so it is the desired object to simulate star images. The wavefront represents the surface of equal phase for light waves passing through the exit pupil of the camera. The Zernike coefficients come from an orthonormal polynomial expansion of the wavefront on the unit disk in terms of the normalized radial coordinate ρ and the azimuthal coordinate θ. *Zemax* outputs the first 37 Zernike coefficients of the wavefront by default. In order to create artificial images of stars, the PSF must be obtained at the location of the focus and alignment CCDs in the model. *Zemax* can output the PSF and wavefront directly into a discrete array, however the Zernike coefficients were used instead. They provide a concise approximation of the wavefront with only 37 numbers, which can then be converted to the PSF via a Fourier transform.

A macro was created in the ZPL language used by *Zemax* to automate the process of extracting Zernike coefficients to text files. Python code already developed by Aaron Roodman was then used to convert the Zernike coefficients to realistic images. The code binned the wavefront into an array and applied a discrete Fourier transform from the SciPy library to convert to a PSF. To finally convert to a realistic image, three more effects needed to be added, atmospheric seeing, pixelation, and noise. Atmospheric seeing can be added by convoluting the pure PSF with the inverse transform of the modular transfer function, $e^{-3.44\left(\frac{r}{r_0}\right)^{5/3}}$, describing the Kolmogorov model of atmospheric turbulence.[3] r_0, called the Fried parameter, expresses the degree of atmospheric seeing. Similarly, pixelation can be incorporated by convoluting the PSF with the box function, defined to be 1 inside a square the same size of a pixel, and 0 elsewhere.[4] Noise can be included by adding two normally distributed random variables; the first is photostatistics noise with a Poisson distribution, and second is read noise of order 10 photons. Finally, using the PyFITS module, a standard astronomical FITS (Flexible Image Transport System) format image can be created. A typical image is shown Figure 3. Note that the hole in the center is due to the obscuration of the camera inside the telescope.

The primary tool and object of study is, of course, the code used to fit images of stars. The code was written in Python and previously written by Aaron Roodman. The code makes use of a number Python libraries located on the KIPAC software directory including NumPy, SciPy, ROOT, PyFITS, and FFTW. The routine was run on a typical Linux desktop at KIPAC. The code was split into two parts. The first

FitFunc, takes an input FITS image, defines constants used in the fit, and provides the machinery used to calculate the parameters to be fitted and the value from the fit. The FFTW (Fastest Fourier Transform in the West) package is used to increase the speed of fitting. The second part, called focusfit, uses the TMinuit package from CERN's ROOT library to perform the minimization for the fit and returns statistical data about the fit, including parameters and errors, a correlation matrix, and the value. The parameters returned by the fit are listed in Table 1. $nPhotons$ represents the total flux of the star received in units of photons (or rather electrons, since that is what is actually counted in a CCD). $xOffset$ and $yOffset$ describe the coordinates of the center of the star in units of pixels. A_d, A_{t_x}, and A_{t_y} are Seidel coefficients of aberration for defocus, and x and y tilt respectively. In addition, the capability to fit for a background and r_0 were added later to accomodate the real images from Mosaic II. The fit works much in the same way that artificial images are created. Using a starting set of Zernike coefficients and the initial parameters given to the fit, a default PSF is created using the same procedure described to create artificial images. Then, as the fit moves through parameter space, the PSF is recalculated as neccessary, and the difference between the real and calculated image is used to calculate a χ^2 value. This fit is unique in that photostatistics Poisson errors plus read noise are used as the errors in the χ^2 formula. The fit iterates this calculation until a minimum χ^2 value is found.

A_d is the coefficient in front of the term proportional to ρ^2 in a series expansion of the wavefront. It is particularly useful since it is related to the shift in position of the camera along the longitudinal axis of the telescope via the formula,

$$A_d = \frac{n}{8F^2\lambda}\Delta z \tag{1}$$

where Δz is the shift in camera position along the longitudinal z axis[1], λ is the wavelength of light, n is the index of refraction (which can be taken to be effectively 1), and F is the f-number, the ratio of the focal length (the distance from the exit pupil to the focal point) to the diameter of the exit pupil.[5] Note that this formula is approximate and only holds for small Δz. $A_{t_x}$and $A_{t_y}$are the coefficients of the terms proportional $\rho\cos\theta$ to $\rho\sin\theta$ respectively. They are useful because they can be related directly to the angle of tilt about the y and x axes respectively, namely they are directly proportional to the angle of tilt by the factor na/λ where a is the radius of the exit pupil of the camera.[6]

For the next test of the fit, images were provided by David Burke from the Mosaic II imager currently installed on the Blanco telescope. Images were taken in a variety of telescope orientations to see if the fit could detect any mechanical fluctuations. For a given telescope orientation, sets of star images were taken using the entire detector plane of Mosaic with a special procedure to gauge the ability to detect shift in the

[1] A note on signs: Here the convention will be used that "plus" means a camera shift toward the primary mirror and "minus" means away from it.

z direction. The camera was placed either plus or minus 1200 microns out of focus. After the first image was taken in such a configuration, the camera was shifted by 100 microns, and the charge on the CCDs was shifted by 200 pixels, maintaing the previous image. Then another image was taken, and the charge was shifted 100 pixels. The same was done 3 more times, so there were 5 images of the same set of stars lined up on the same CCD, spaced by increments of 200-100-100-100 pixels. A typical set of 5 images of the same star is shown in Figure 4. The first 200 pixel shift is done so there is a way of determining which of the images of the same star was taken first. Additionally, in-focus images were taken to test the abilities to detect variations in tilt. To handle the real images, some changes needed to be made to the fitting code. All images have a background level, so the capability to fit for a constant background was added. In addition, the r_0 fluctuates considerably over time, so it is beneficial to fit for it as well. After flat-fielding the images and cutting out individual star images into square "postage stamps", they are ready to fit.

Results

To quantify the reliability of the algorithm to detect defocus, i.e. shifts in z position along the longitudinal axis of the telescope, plots of A_d vs. Δz were made and the slope of a linear fit compared to the theoretical value $\frac{n}{8F^2\lambda}$ predicted by (1). The F number used in this formula was obtained from *Zemax* and has a value of 2.990 for DECam and 2.908 for Mosaic II. For artificial images, an average wavelength of $\lambda = 756$ nm was used to create the image. For images from Mosaic II, the filter used has a central value of $\lambda = 644$ nm.[7] Issues regarding the use of these numbers will be discussed later.

Using the *Zemax* model of DECam and the Blanco Telescope, images were created in the vicinity of the focus and alignment sensors at ± 1.5 millimeters out of focus with 20 micron increments in Δz. The images were fit, and the values of A_d returned by the fit were plotted against the shifts in z used in the *Zemax* model. The plots are shown in Figures 5 and 6 along with statistical data. Similarly, the same procedure was done for sets of 5 star images taken from Mosaic II. An example of fitting A_d vs. Δz for a set of star images at $+1.2$ mm out of focus and moving out of focus by steps of 100 microns is shown in Figure 7. (This is the same set of stars as shown in Figure 4.) An example of the data returned by the fit of a single image is shown in Table 1, in this case the first star image in Figure 4. Figure 8 shows the calculated best-fit image, a difference image between the calculated and real images, and the real image of a single star, the same as was fitted from Table 1. Table 2 shows the value of the slope of A_d vs. Δz for fits of star image sets at both plus or minus 1200 microns. The value of r_0 returned by the fit of the first star image and the measured value of r_0 at the time the image was taken are shown in Table 3 for both sets plus and minus 1200 microns out of focus.

Conclusions

The A_d vs. Δz fits of artificial images in Figures 5 and 6 show an excellent linear fit, but the slope is strangely high for both cases. However, the slopes produced by both are consistent. The A_d vs. Δz plot in Figure 7 from the Mosaic image does show a linear relationship, however, the high χ^2 value indicates there is a systematic effect that is not being taken account. This is universal of all star sets from Mosaic so far fitted. Table 2 shows that the slope of A_d vs. Δz is being consistently being overestimated regardless of location. The excessive slope therefore seems to be a plague of all fits. Either the value of $\frac{n}{8F^2\lambda}$ being used as comparison is wrong or there is a disease on the algorithm that must be found. The simple formula from (1) can be ambiguous. An 8 wavelength set from 700 nm to 825 nm in *Zemax* was used to create artificial images, and the average wavelength was used in (1). This may be a false assumption. Similarly, the red filter used on Mosaic to take images extends over a relatively large range of wavelengths of FWHM 151 nm (a transmission diagram illustrates this in Figure 9).[8] The central wavelength was used in (1), however this may also be false. Also problematic may be the f-number. *Zemax* returns the effective f-number of the entire optical system; however, it is the f-number of the light cone converging on the focal point to which (1) refers.

Furthermore, there is a clear pattern to the difference plot shown in Figure 8. This pattern is persistent for each image in a set of 5, but it is unique to each set of images. What systematic effect causes these difference pattern needs to be investigated. This will lead to an improvement of fit quality for all sets of images, which all seem to share similarly poor χ^2 values so far. Finally, Table 3 shows that the fit consistently does not estimate r_0 to within the error bounds returned, which may be related to unmodeled systematic effects discussed before or it may be that the fit is not sensitive to fitting for r_0.

To summarize the problems and future issues:

1. Why are the fits of real images so poor? What effect is not being modeled by the fit?
2. In fits from real images, what causes the large deviations from the theoretical straight line relation for A_d vs. Δz as well as deviations from the measured values of r_0? Why is the slope of A_d vs. Δz consistently larger than expected?
3. Investigations of the reliability of the tilt coefficients A_{t_x} and A_{t_y} have yet to be done.
4. Heretofore not mentioned, timing is a critical issue as focus and alignment data will be used after every other image, which will be read out in approximately 17 seconds and have exposure times of ≈ 100

seconds[9]. Currently, fits of real images take 3 to 6 minutes to complete. Optimization strategies will have to be investigated.

Each of these problems will require further work; however, the method itself is very promising. The development of the algorithm is only in its beginning stages, and much more work needs to be done to realize its full potential.

Acknowledgments

This work was conducted at SLAC National Laboratory and supported by the United States Department of Energy, Office of Science and SLAC. Thanks go to my mentor Aaron Roodman for his generous guidance, patience, and support, David Burke for collecting the data from Mosaic II and providing support in analyzing that data, Reyna Garcia for preparing images for fitting, and the SULI staff who work to make the program run smoothly.

Literature Cited

[1] "The Dark Energy Survey Science Program," [Online]. Available: http://web.hep.uiuc.edu/home/jjt/DES_docs/DES_Science_Program.pdf. [Accessed: Aug. 12, 2009].

[2] "Instrument," *Dark Energy Survey Data Managment*, [Online]. Available: http://cosmology.uiuc.edu/DES/desproject/instrument.html. [Accessed: Aug. 12, 2009].

[3] D. J. Schroeder, *Astronomical Optics*, 2nd ed. San Diego: Academic Press, 2000, pp. 412.

[4] D. J. Schroeder, *Astronomical Optics*, 2nd ed. San Diego: Academic Press, 2000, pp. 427.

[5] V. N. Mahajan, *Aberration Theory Made Simple*, New York: SPIE-International Society for Optical Engineers, pp. 9.

[6] V. N. Mahajan, *Aberration Theory Made Simple*, New York: SPIE-International Society for Optical Engineers, pp. 10.

[7] "CTIO Mosaic II Imager User Manual," *Cerro Tololo Inter-American Observatory*, [Online]. Available: http://www.ctio.noao.edu/mosaic/manual/index.html. [Accessed: Aug. 12, 2009].

[8] "CTIO Mosaic II Imager User Manual," *Cerro Tololo Inter-American Observatory*, [Online]. Available: http://www.ctio.noao.edu/mosaic/manual/index.html. [Accessed: Aug. 12, 2009].

[9] "Instrument," *Dark Energy Survey Data Managment*, [Online]. Available: http://cosmology.uiuc.edu/DES/desproject/instrument.html. [Accessed: Aug. 12, 2009].

Figures and Tables

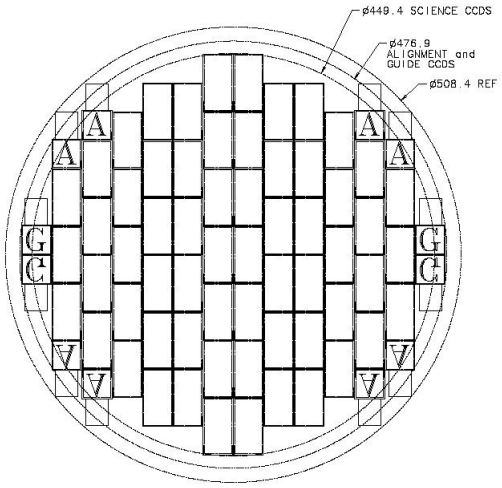

Figure 1: The focal plane of DECam; the focus and alignment sensors are indicated by the letter A.

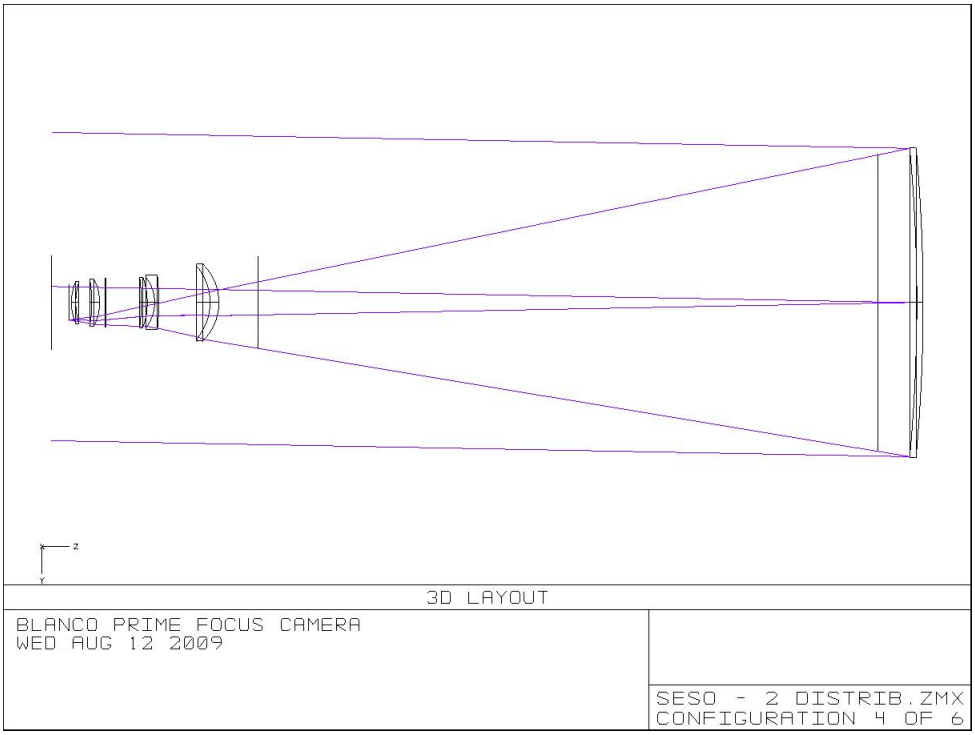

Figure 2: A diagram of DECam and Blanco in *Zemax* also depicting rays converging on a focus and alignment sensor.

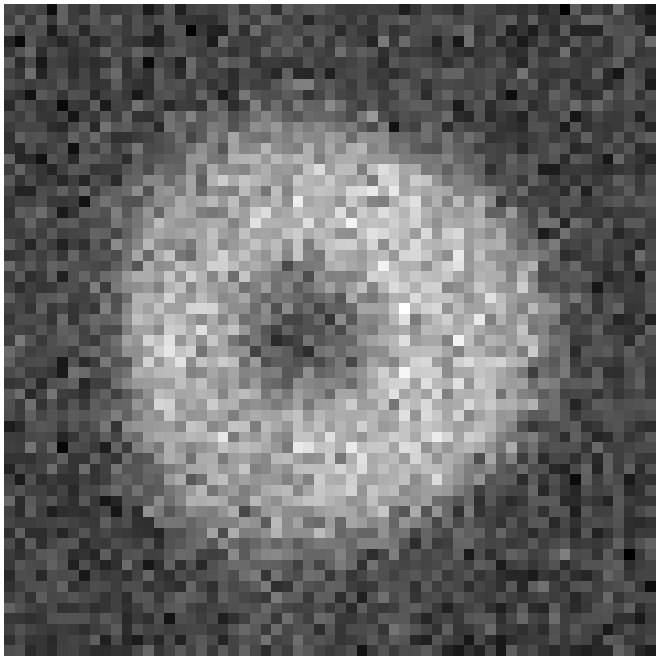

Figure 3: An artificial star image created at a sensor 1.5 mm below the focal plane, while the camera was in-focus.

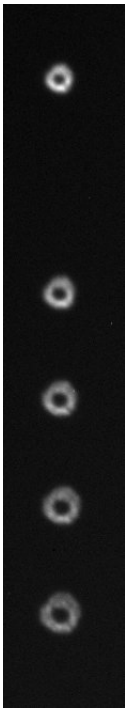

Figure 4: A cutout of a set of 5 star images from Mosaic II at +1.2 mm out of focus and moving further out of focus by increments of 100 microns. Many sets of 5 star images are found on every CCD.

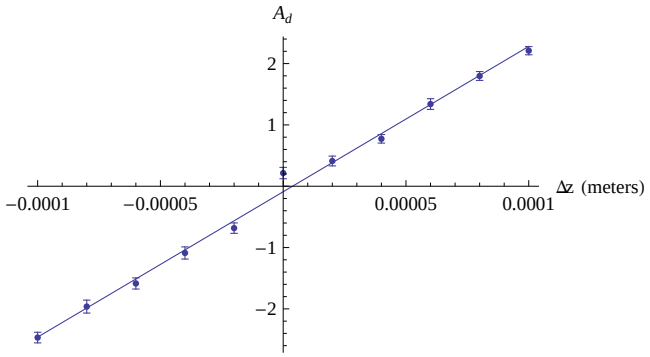

a	$b(\mathrm{m}^{-1})$	$\frac{n}{8F^2\lambda}$ (m^{-1})	$\frac{\chi^2}{n-2}$
-0.102636 ± 0.0339515	23562.8 ± 519.104	18494.6	1.77602

Figure 5: A linear fit of A_d vs. Δz to $a + bx$ with images from one of the focus and alignment sensors +1.5 mm above the focal plane.

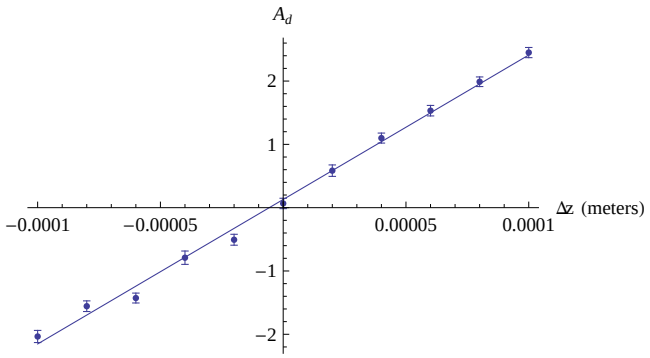

a	$b(\mathrm{m}^{-1})$	$\frac{n}{8F^2\lambda}$ (m^{-1})	$\frac{\chi^2}{n-2}$
0.124069 ± 0.0338838	23022.7 ± 531.66	18494.6	1.75718

Figure 6: The same plot as in Figure 5 only with images taken from a sensor 1.5 mm below the focal plane.

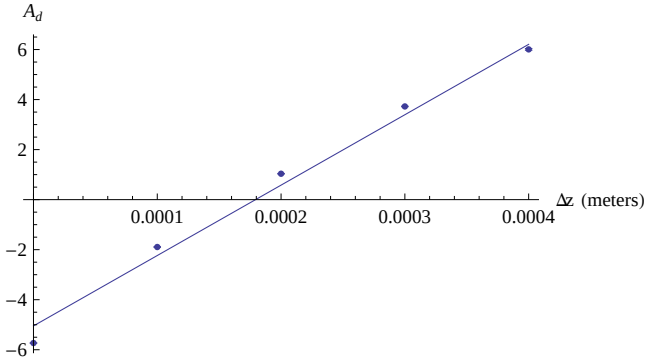

a	$b(\mathrm{m}^{-1})$	$\frac{n}{8F^2\lambda}$ (m^{-1})	$\frac{\chi^2}{n-2}$
-5.45017 ± 0.303405	31082.0 ± 1587.32	22952.8	1.75718

Figure 7: A fit of A_d vs. Δz from Mosaic II with the camera starting from +1.2 mm out of focus.

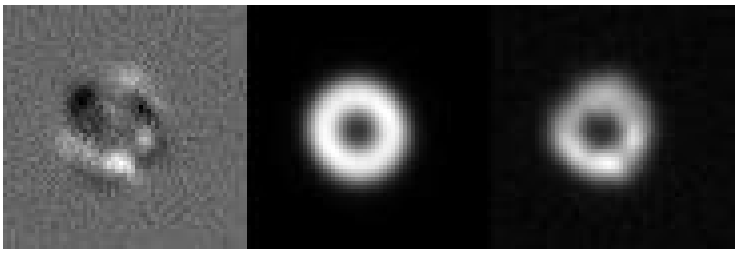

Figure 8: The difference image, the best-fit calculated image, and the actual image for the first image of the star set shown in Figure 3.

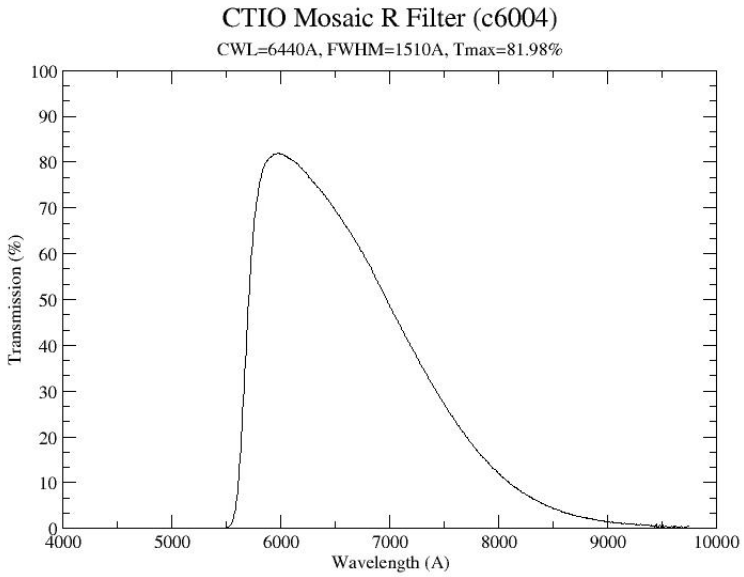

Figure 9: The transmission diagram for the red filter used on Mosaic II.

Correlation Matrix	$nPhotons$	$xOffset$	$yOffset$	A_d	A_{t_x}	A_{t_y}	r_0	$bkgd$
$nPhotons$	1	-0.013	-0.013	0.160	0.015	0.022	-0.535	-0.492
$xOffset$	-0.013	1	-0.026	-0.094	0.002	-0.030	-0.011	0.008
$yOffset$	-0.013	-0.026	1	-0.004	-0.001	-0.003	0.023	0.008
A_d	0.160	-0.094	-0.004	1	-0.178	0.216	0.129	-0.099
A_{t_x}	0.015	0.002	-0.001	-0.178	1	0.760	-0.144	-0.010
A_{t_y}	0.022	-0.030	-0.003	0.216	0.760	1	-0.055	-0.014
r_0	-0.535	-0.011	0.023	0.129	-0.144	-0.055	1	0.333
$bkgd$	-0.492	0.008	0.008	-0.099	-0.010	-0.014	0.333	1

Parameter	Value	Error
$nPhotons$	2.34314×10^6	3.33661×10^3
$xOffset$	1.77510	1.42374×10^{-2}
$yOffset$	5.48489	1.38277×10^{-2}
A_d	-5.73230	1.00898×10^{-2}
A_{t_x}	-5.47409×10^{-1}	2.92589×10^{-2}
A_{t_y}	6.22443×10^{-1}	2.80884×10^{-2}
r_0	0.974637×10^{-2}	2.96489×10^{-4}
$bkgd$	5.28672×10^3	1.43845

Table 1: The data returned by a typical fit, in this case that of the first image of Figure 3. The χ^2 value of this fit was 25396.7.

Slope of A_d vs. Δz (m^{-1})	Location
31082.0 ± 1587.33	+1.2 mm
25962.3 ± 1874.5	+1.2 mm
27663.0 ± 1264.1	+1.2 mm
32062.4 ± 1264	−1.2 mm
29736.0 ± 1189.2	−1.2 mm

Table 2: Slopes from A_d vs. Δz fits at a variety of locations. The expected value is.

Starting r_0 (m)	Measured r_0 (m)
0.09746 ± 0.00030	0.1244
0.1137 ± 0.0048	0.1301
0.1223 ± 0.0050	0.1301
0.12163 ± 0.00034	0.1211
0.09811 ± 0.00065	0.1384

Table 3: Values of r_0 from the fit of the first star image at several locations and measured r_0 values from the time of observation.